Journal of Structural Biology: X 9 (2024) 100099

Contents lists available at ScienceDirect

Journal of Structural Biology: X

journal homepage: www.sciencedirect.com/journal/journal-of-structural-biology-x

# The parabasal filaments of *Trichomonas vaginalis*: A new filament and observations using 0.8 nm-resolution scanning electron microscopy

Sharmila Fiama das Neves Ortiz [a], Raphael Verdan [a], Gustavo Miranda Rocha [b], Kildare Miranda [a,c,d,f], Marlene Benchimol [c,d,e,*]

[a] *Laboratório de Ultraestrutura Celular Hertha Meyer, Instituto de Biofísica Carlos Chagas Filho, Universidade Federal do Rio de Janeiro, Rio de Janeiro, Brazil*
[b] *Unidade de Pesquisa Urogenital, Centro Biomédico, Departamento de Anatomia, Universidade Estadual do Rio de Janeiro, Rio de Janeiro, Brazil*
[c] *CENABIO - Centro Nacional de Biologia Estrutural e Bioimagem, Universidade Federal do Rio de Janeiro, Rio de Janeiro, RJ, Brazil*
[d] *Instituto Nacional de Ciência e Tecnologia em Biologia Estrutural e Bioimagem – Universidade Federal do Rio de Janeiro, Rio de Janeiro, Brazil*
[e] *UNIGRANRIO-Universidade da Grande Rio, Rio de Janeiro, Brazil*
[f] *Centro Multiusuário para Análise de Fenômenos Biomédicos, Universidade do Estado do Amazonas, Manaus, Brazil*

ARTICLE INFO

*Keywords:*
Cytoskeleton
Trichomonads
New filament
Striated fibers
Fast Fourier transform
Tomography

ABSTRACT

*Trichomonas vaginalis* is the etiologic agent of trichomoniasis, the most common nonviral sexually transmitted infection worldwide, with an estimated 260 million new cases annually. *T. vaginalis* contains organelles common to all eukaryotic cells, uncommon cell structures such as hydrogenosomes, and a complex and elaborate cytoskeleton constituting the mastigont system. The mastigont system is mainly formed by several proteinaceous structures associated with basal bodies, the pelta-axostylar complex made of microtubules, and striated filaments named the costa and the parabasal filaments (PFs). Although the structural organization of trichomonad cytoskeletons has been analyzed using several techniques, observation using a new generation of scanning electron microscopes with a resolution exceeding 1 nm has allowed more detailed visualization of the three-dimensional organization of the mastigont system. In this study, we have investigated the cytoskeleton of *T. vaginalis* using a diverse range of scanning probe microscopy techniques, which were complemented by electron tomography and Fast-Fourier methods. This multi-modal approach has allowed us to characterize an unknown parabasal filament and reveal the ultrastructure of other striated fibers that have not been published before. Here, we show the differences in origin, striation pattern, size, localization, and additional details of the PFs, thus improving the knowledge of the cell biology of this parasite.

## Introduction

*Trichomonas vaginalis,* the agent of human trichomoniasis, is a common sexually transmitted infection that can provoke reproductive tract inflammation, adverse pregnancy outcomes, an increased risk of HIV and other vírus infections, and cervical or prostate cancer. In addition to its importance in medicine, *T. vaginalis* is a good model for studying uncommon cell structures. Besides the organelles found in all eukaryotic cells, such as the nucleus, endoplasmic reticulum, Golgi, and lysosomes, it contains hydrogenosomes and a complex and elaborate cytoskeleton, constituting the mastigont system (Benchimol, 2004, 2010; Honigberg et al., 1971). *T. vaginalis* has four anterior flagella (AF) and one recurrent flagellum (RF) attached to an undulating membrane (Fig. 1). The mastigont system comprises a well-organized array of microtubules, known as the pelta-axostylar complex, which constitutes an axial skeleton formed by stable, longitudinally oriented microtubules and extends across the length of the cell. The pelta reinforces the wall of the flagellar canal from which the five flagella emerge (Honigberg et al., 1971). The axostyle promotes the axial support of the cells and participates in karyokinesis during cell division (Ribeiro et al., 2000). In addition, many fibers are not yet well characterized, either in ultrastructure or function, such as the sigmoidal and parabasal filaments (PFs). Around the basal bodies are several appendages and rootlet filaments forming a poorly studied complex accessory system.

Trichomonads possess a large and major striated root fibril linked to the undulating membrane, known as costa, that is thought to provide mechanical support to this structure. It originates from the second basal body and passes under the recurrent flagellum's basal body, exhibiting

* Corresponding author at: CENABIO - Centro Nacional de Biologia Estrutural e Bioimagem, Universidade Federal do Rio de Janeiro, Rio de Janeiro, RJ, Brazil.
*E-mail addresses:* marlenebenchimol@gmail.com, marlenebenchimol@biof.ufrj.br (M. Benchimol).

https://doi.org/10.1016/j.yjsbx.2024.100099
Received 28 February 2024; Accepted 4 March 2024
Available online 6 March 2024

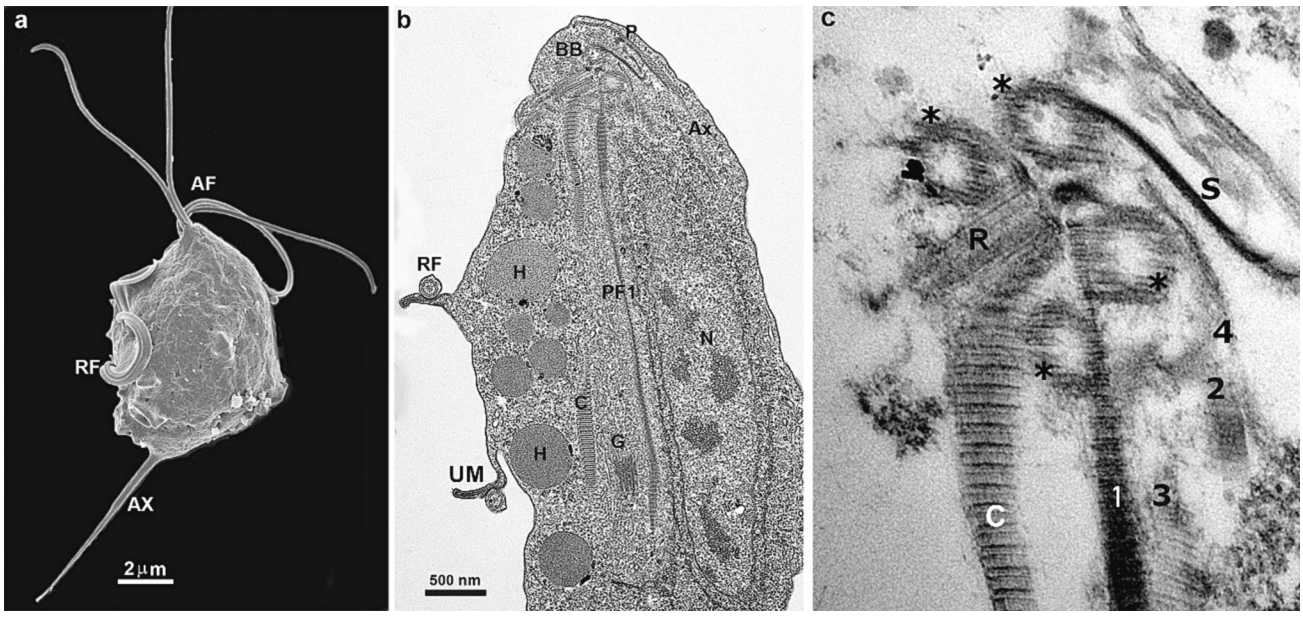


**Fig. 1.** General view of *T. vaginalis* in high-resolution SEM (a) and transmission electron microscopy (TEM) of the whole cell (b) and the isolated cytoskeleton (c). AF, anterior flagella; RF, recurrent flagellum; Ax, ax style; H, hydrogenosomes; N, nucleus; G, Golgi; BB and asteriscs, basal bodies of the flagella; C, costa; R, basal body of the recurrent flagellum; P, pelta; S, sigmoidal filament; and Parabasal filaments (PF) numbered from 1 to 4.

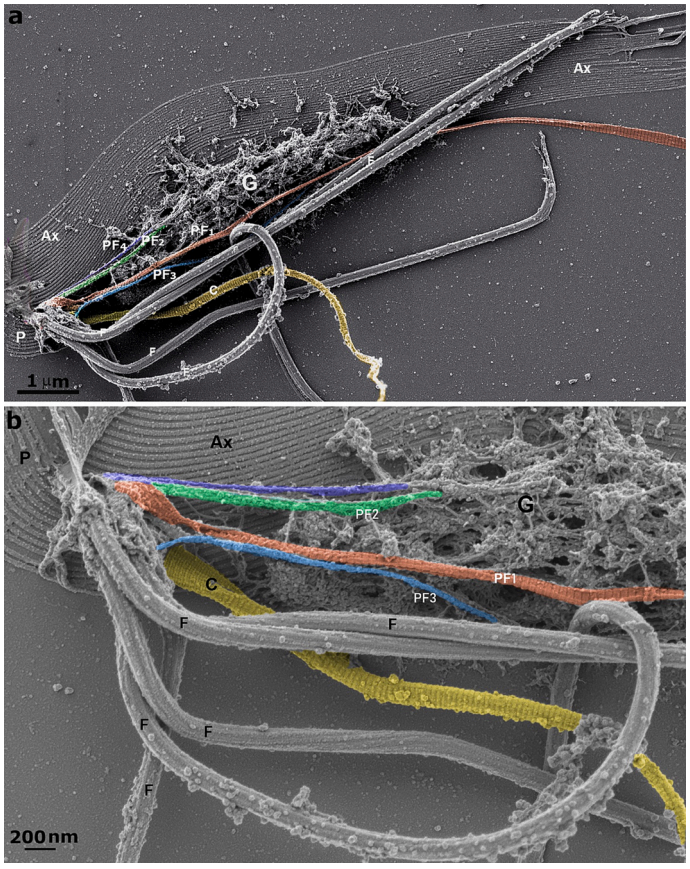


**Fig. 2.** UHR SEM of the isolated cytoskeleton of *T. vaginalis* in low (a) and higher magnification (b). The four striated fibers are colored orange (PF1), green (PF2), blue (PF3), and purple (PF4). Notice a remnant of a probable Golgi. PF1 and PF3 run on the *cis*-Golgi face, whereas PF2 and PF4 run on the *trans*-Golgi's face. The costa (C) is colored in yellow. Notice that PF1 is the longest fiber accompanying the axostyle (Ax). Flagella (F), Golgi (G), Pelta (P).

periodicity and alternate wide and thin bands with a complex array of filaments (Benchimol, 2004). The costa is associated with the hydrogenosomes, an organelle that produces ATP in trichomonads since this parasite does not have mitochondria.

Other striated fibers in this protist are the parabasal filaments, thinner than the costa, with distinct periodicity and patterns. They are

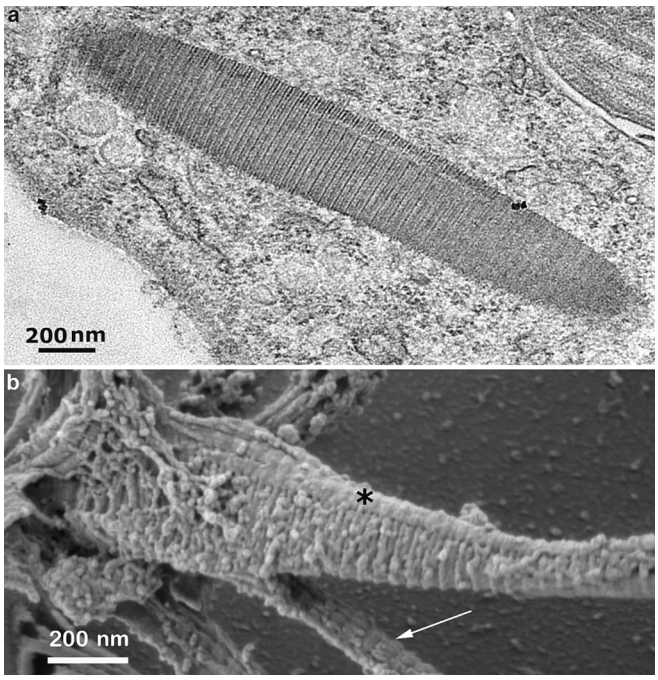


**Fig. 3.** Transmission electron microscopy (a) and UHR-SEM (b) of costa of *T. vaginalis*. In ultrathin sections, it is possible to see the periodicity. (b) It is possible to observe the intricate mesh of several filaments that forms the sub-structure of the costa using UHR-SEM. Notice that in the periphery (asterisk), there is a difference in its structure. A parabasal filament is seen running behind the costa (arrow).

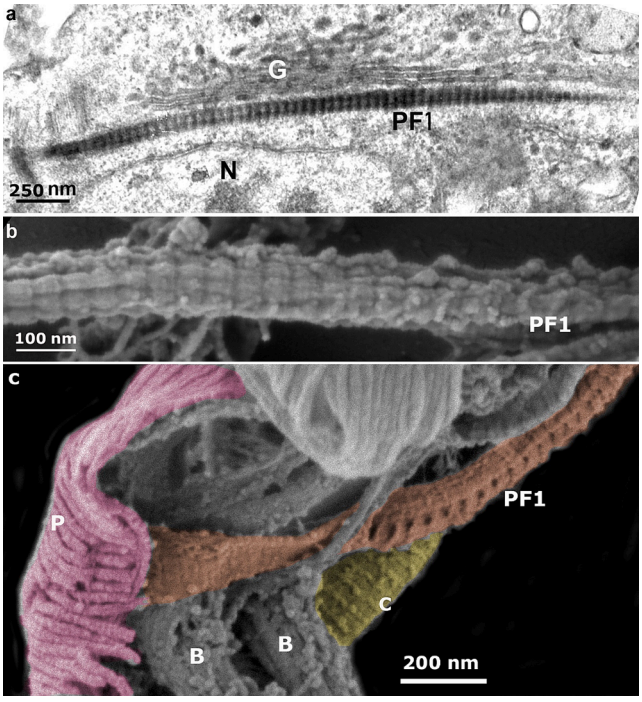


**Fig. 4.** The parabasal filament 1 (PF1) is seen in three situations: (a) in a thin section observed in TEM and (b-c) in UHR-SEM. Notice in (b) that its surface presents marks; in (c), the fiber seen from below shows a distinct pattern. Pelta (P) microtubules in pink. B, basal body (kinetosome); C, costa.

believed to connect the basal bodies to the first Golgi cisternae, possibly to support this organelle (Honigberg and Brugerolle, 1990).

Due to this association, the Golgi in Trichomonads is named

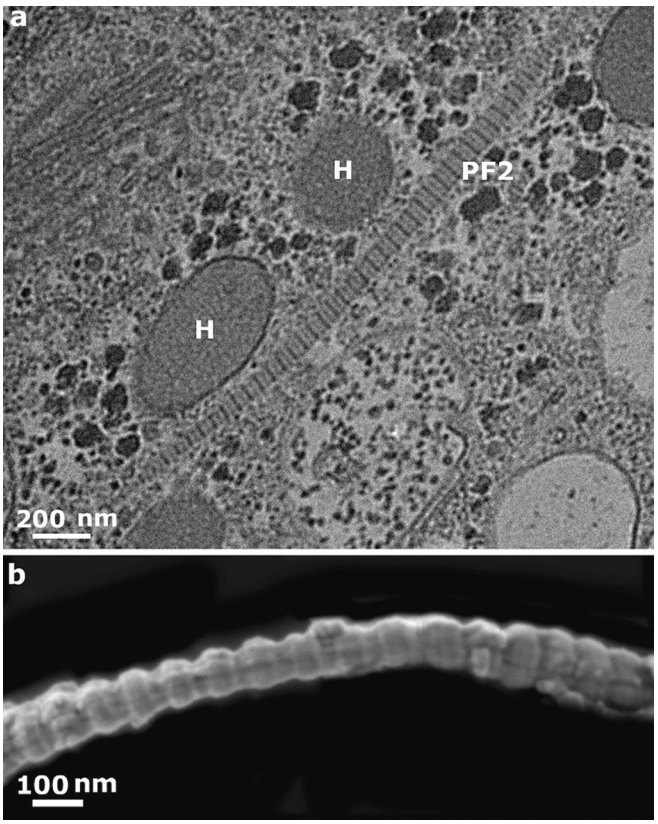


**Fig. 5.** Transmission electron microscopy (a) and UHR-SEM (b) of parabasal filament 2 (PF2) of *T. vaginalis*. H, hydrogenosome.

parabasal apparatus (Honigberg and Brugerolle, 1990; Benchimol et al., 2001).

There is a controversy in the literature in which some authors describe two parabasal filaments (Cepicka et al., 2016), while others describe three parabasal filaments (Lee et al., 2009).

Although complex, many of these structures are poorly studied, and their functions remain an enigma. Despite providing excellent images with great resolution, the transmission electron microscope has the disadvantage of sectioning the cells into very thin slices, which leads to the loss of information in 3-D. Thus, we present new detailed images of the parabasal filaments using cutting-edge techniques. Electron tomography microscopy emerged as a powerful tool for comprehensively elucidating intricate three-dimensional structures within various cellular models, including parasitic organisms. Despite the versatility of these methods, there remains a notable absence of studies employing tomographic analyses specifically geared toward examining *Trichomonas vaginalis*, highlighting an untapped potential for applying this advanced imaging technique. Electron tomography microscopy enables researchers to delve into the intricate structural details of biological specimens, providing a three-dimensional perspective that surpasses the limitations of traditional two-dimensional imaging. The technique involves acquiring a series of images from multiple angles, allowing for the reconstruction of a detailed 3D model (Brown et al., 2016; Trépout et al., 2018).

There is a controversy in the literature in which some authors describe two parabasal filaments (Čepička et al., 2016). In contrast, others claim three distinct parabasal filaments in *T. vaginalis,* where one split (Lee et al., 2009).

More recently, a considerable improvement in scanning electron microscopy images was the introduction of the UHR-SEM, which allowed high-resolution images of below 1 nm using only a very thin platinum coating. It produces images with resolution comparable to

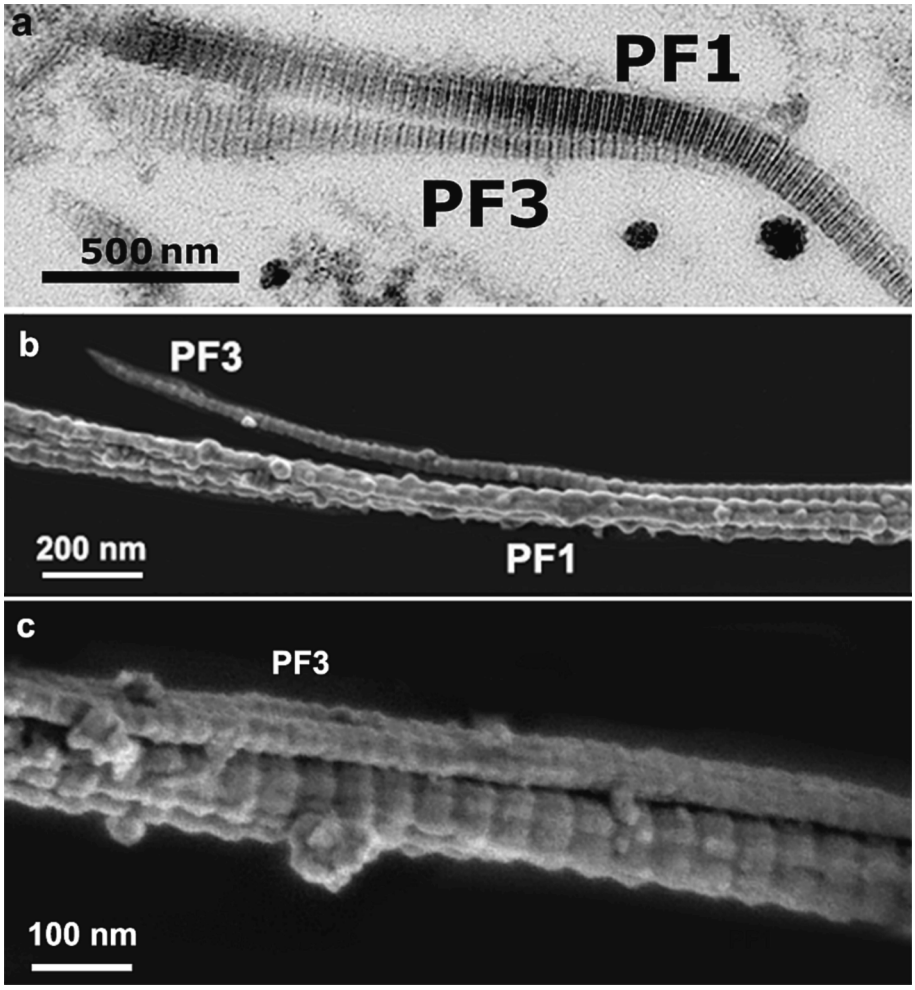


**Fig. 6.** Transmission electron microscopy of the isolated cytoskeleton of *T. vaginalis*, showing in (a) the parabasal filament 3 (PF3). (b-c) UHR-SEM of PF1 and PF3. Note the proximity of these striated filaments and that, at a certain point, PF3 separates and becomes thinner.

transmission electron microscopy (TEM), with 3-D views. It allows the observation of previously unseen cell structures, such as detailed views of the trichomonad cytoskeleton and the fibril anchorage. In addition, appropriate buffers and detergent extraction procedures removed the plasma membrane and exposed the cell's interior, allowing the visualization of organelles and cytoskeleton impressively.

This study analyzed *T. vaginalis* structures with UHR-SEM after extracting the plasma membrane. Thus, we could visualize the cell interior and the main skeletal structures.

We optimized a detergent-based extraction protocol to obtain an enriched fraction of the *T. vaginalis* cytoskeleton (Viscogliosi and Brugerolle, 1994; De Andrade Rosa et al., 2013; Preisner et al., 2016; De Souza and Cunha-e-Silva, 2003). The success of the extraction was confirmed through light microscopy.

We can establish correlations between our tomography findings by employing a powerful scanning electron microscope (SEM), which facilitates visualization of structures at smaller scales. Traditionally, SEM images reveal the surface of cells and organisms. However, with the advent of very high-resolution microscopes, it was possible to observe the inside of cells after removing the plasma membrane and various organelles with detergents. We used the Auriga-SEM operating between 100 V and 30 kV, which gives resolutions of 1.0 nm at 15 kV and 1.9 nm at 1 kV. In addition, the gold coating was not used, which allowed a closer natural view of the cell's structures. In this way, the cytoskeleton and remnants of the organelles could be visualized in a three-dimensional view, a fact that had not been seen since then. The correlation of SEM images with those of Atomic Force Microscopy (AFM) brings new aspects of morphology that were not demonstrated before, particularly when characterizing structures at the nanometric scale in periodicity (Dvorak et al., 2000; Rocha et al., 2010). In addition, Fast Fourier Transform analyses are important since they transform spatial information into frequency space, revealing periodic patterns otherwise inviable in direct imaging. The interplay between these techniques is essential for elucidating very small structures that pose challenges in visualization.

## Materials and methods

### *In vitro culture of T. vaginalis*

*T. vaginalis*, strain JT, was isolated from a patient attending the Rio de Janeiro Federal University Hospital. *T. vaginalis* isolate 347 + was provided by Dr. Alderete and was also used. The cells were cultivated in trypticase yeast-extract maltose medium, TYM Diamond's (Diamond, 1957), supplemented with 10 % fetal calf serum. Cultures were maintained in Falcon's ® tube of 15 mL at 37 °C and subcultured daily.

### *T. vaginalis cytoskeleton isolation*

The trophozoites from a confluent culture were detached from the tube wall by placing it on ice for 15 min, followed by centrifugation at 1,000 g for 5 min. The cells were washed twice with phosphate-buffered

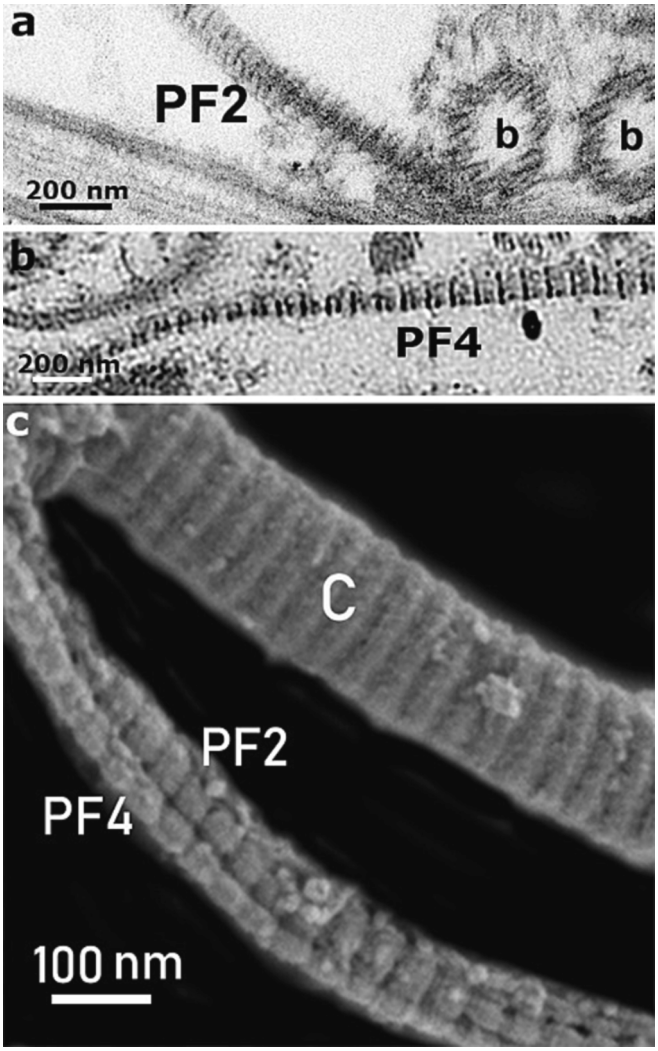


**Fig. 7.** Transmission electron microscopy (a-b) and UHR-SEM (c) of parabasal filaments PF2 and PF4. Note the differences in periodicity and thickness. C, costa.

saline (PBS) at pH 7.2 at room temperature (RT) and centrifuged. For the cytoskeleton extraction, the cells were then resuspended with 2 mL ice-cold extraction solution containing PHEM buffer (60 mM PIPES, 25 mM HEPES, 10 mM EGTA, and 4 mM $MgSO_4 \cdot 7H_20$) containing 30 % glycerol (Sigma Aldrich, EUA), 2 % Triton X-100 (Sigma Aldrich, USA), 2 % Igepal (Sigma Aldrich, USA) including one 1x protease inhibitor cocktail (Sigma Aldrich, USA). The cells in the extraction solution were incubated on ice for 2 min, vigorously vortexed at maximum speed for two minutes, and repeated twice. Then, the cytoskeleton-enriched fraction was washed in 1 mL of PBS pH 7.2 and centrifuged at 17,000 x g for five minutes at 4 °C. The success of the extraction was confirmed through light microscopy. The samples were fixed according to each microscopy routine procedure.

*Scanning electron microscopy (SEM) and 0.8 nm - resolution SEM (UHR-SEM)*

In routine processing for scanning electron microscopy, the cytoskeleton-enriched fraction was fixed in 1 mL 2.5 % glutaraldehyde (Electron Microscopy Sciences, USA) in 0.1 M cacodylate buffer, pH 7.2. Then, they were post-fixed with 1 % osmium tetroxide ($OsO_4$) in 0.1 M phosphate buffer, pH 7.2, and 0.8 % potassium ferricyanide for 30 min and dehydrated in increasing concentrations of ethanol (15 min in each concentration). The samples were dried by the critical point method (Leica CPD 300, Germany), mounted on metallic supports (stubs), and coated with 10 nm of gold, depending on the SEM used for the analyses (Quanta 250 (FEI, Netherlands) operating at 20 kV.

For 0.8 nm-resolution SEM, the samples were fixed and dehydrated as above, dried by the critical point method (Leica CPD 300, Germany), mounted on metallic supports (stubs), and coated with 2–4 nm platinum and observed on an Auriga 40 SEM (Zeiss, Germany) operating at 2 kV. Images were acquired with a 1.0–3.0 mm working distance.

*Transmission electron microscopy (TEM)*

Samples were washed in PBS, pH 7.2, and subsequently fixed in 1 mL of 2.5 % glutaraldehyde (Electron Microscopy Sciences, USA) in 0.1 M cacodylate buffer, pH 7.2. The cells were washed in PBS and post-fixed in a solution containing 1 % $OsO_4$ in 0.1 M phosphate buffer, pH 7.2, and 0.8 % potassium ferricyanide for 30 min without light. After the post-fixation step, the samples were washed three times in PBS again. Then, the cells were dehydrated in acetone solution, gradually infiltrated with an epoxy resin, and polymerized at 60 °C for 72 h. Thin sections were stained with uranyl acetate and lead citrate and visualized under a Hitachi HT 7800 transmission electron microscope (Japan).

*Negative staining*

For the first step, we dropped 1 % of the cytoskeleton-enriched fraction in PBS onto glow-discharged and formvar-coated copper grids. The grids were then rinsed in PEME buffer (100 mM PIPES, 1 mM $MgSO_4$, 0.1 mM EDTA, and 2 mM EGTA, pH 6.9) for 5 min and fixed with 10 μl of 2.5 % glutaraldehyde in PEME for 5 min at RT and subsequently negatively stained with 1 % aurothioglucose (Sigma-Aldrich, USA) in water ice-cold temperature (adapted from Vidal et al., 2016). Observations were made in a Hitachi HT 7800 transmission electron microscope (Japan).

*Atomic force microscopy (AFM)*

*Sample preparation and imaging*

For sample preparation, 80 μl of the cytoskeleton-enriched fraction in PBS was dispensed onto coverslips, gently rinsed with a pipette, and dried using a low-pressure stream of gaseous nitrogen. Samples were observed using a Bruker Dimension Icon (Santa Barbara, USA). Images were acquired in the air using Peak Force Tapping Mode with 512 × 512 pixels of resolution, and image processing (line-wise flatten only) was performed in NanoScope Analysis 3.0 (Santa Barbara, USA). For better topographic visualization, height images were displayed as 3D views.

*Tomography*

The isolated cytoskeletons were processed for TEM as above. Sections about 350 nm thick were obtained and placed on special open 100 mesh copper grids (Electron Microscopy Sciences, USA), covered with Formvar (Sigma-Aldrich, USA). Samples were post-stained with 5 % uranyl acetate and lead citrate, incubated with 10 nm colloidal gold on both sides for 5 min, and washed in distilled water. A 120-kV transmission electron microscope (Tecnai Spirit, ThermoFisher Scientific, USA) was used for observation. A tilt series from −55° to + 55° with an angular increment of 2° was used for single-axis tomography. Alignments were applied using patch tracking and weighted back projections with the IMOD software package (University of Colorado, USA). We analyzed and constructed 3D models of single-tilt tomograms using the software Amira 5.3.3 (Thermo Fischer, USA). We segmented the features of interest on consecutive optical slices extracted from the tomograms using threshold segmentation. Furthermore, we visualized and rotated the 3D model to examine their three-dimensional geometry.

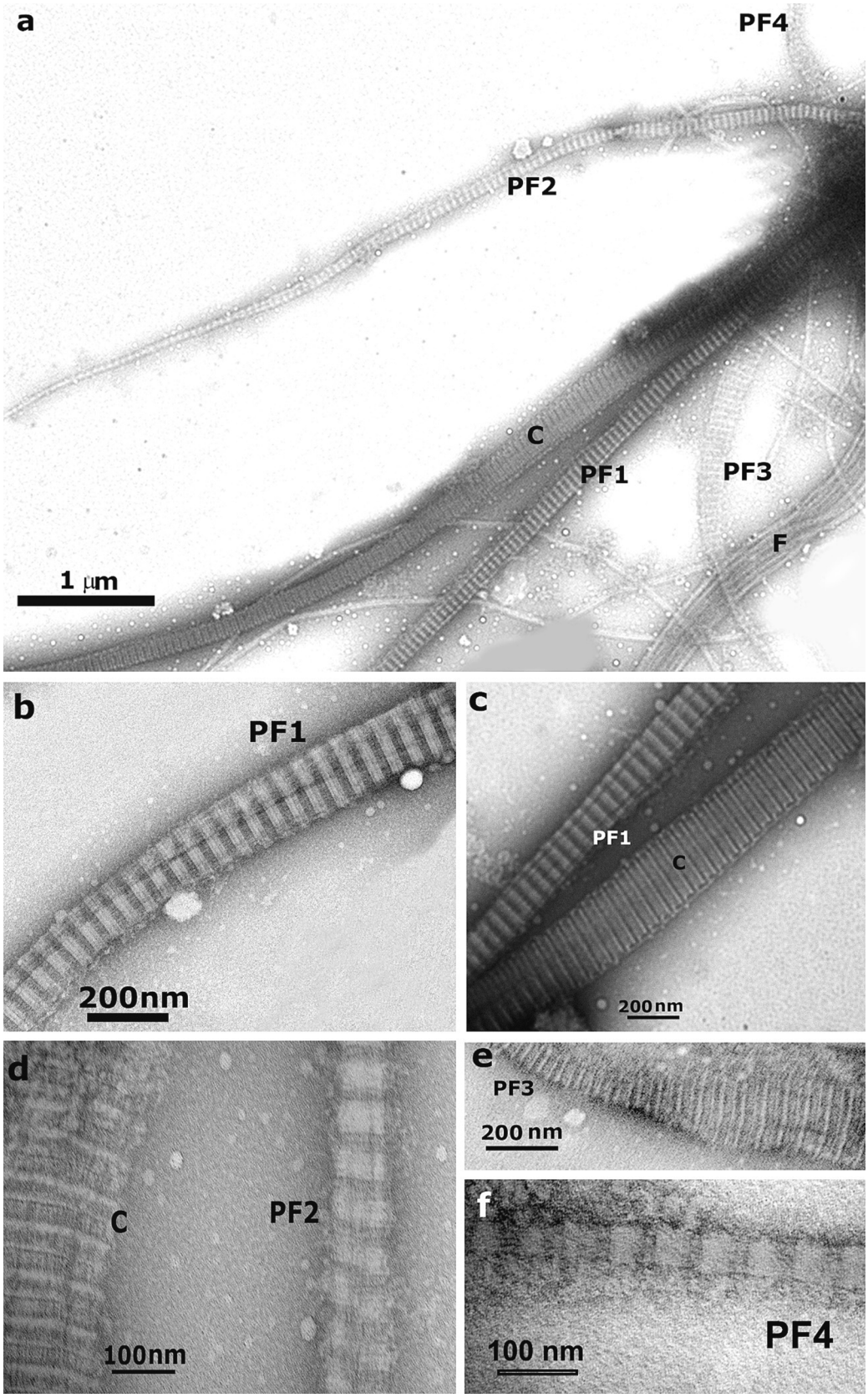


**Fig. 8.** Negative staining of *T. vaginalis* cytoskeleton. The costa (C) presents a different structure and periodicity pattern than other striated filaments (PF1, PF2, PF3, and PF4).

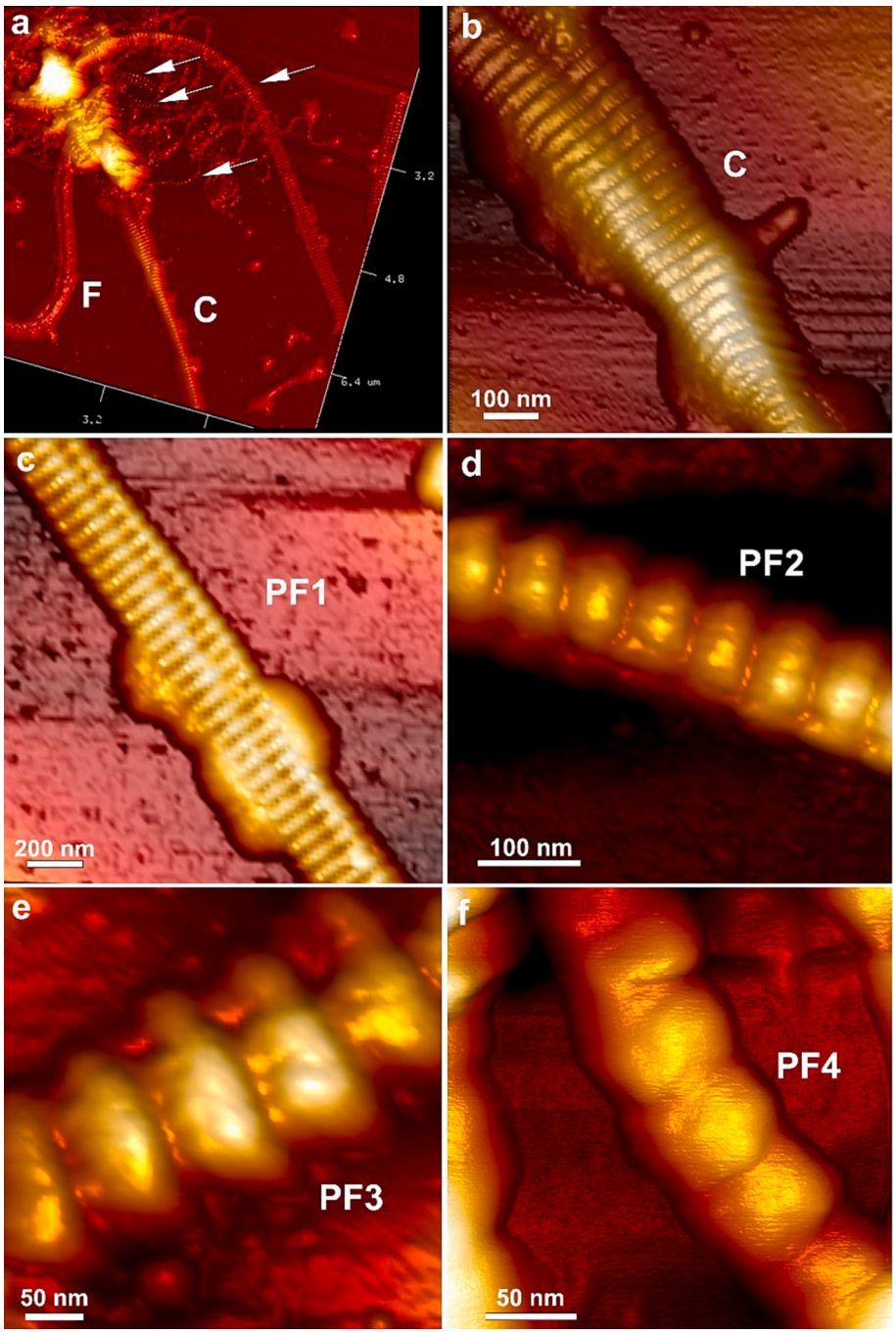


**Fig. 9.** Atomic force microscopy. In (a), an overview of the isolated cytoskeleton of T. vaginalis. The white arrows point to the striated fibers. In (b) costa, and (c, d, e, f), the striated patterns of PF1, PF2, PF3, and PF4 filaments. C, costa; F; flagella.

*Morphometrical analysis*

At least 300 cells of parasites for each condition were examined by scanning electron microscopy to analyze the striated fibers and the parasite surface. The diameter of fibers was measured directly in the scanning electron microscope screen using ZEISS SmartSEM software. We measured using HR-SEM because this equipment allows a whole view of each fiber. We did not include the measurements in TEM because thin sections may give errors since the section does not get the whole fiber, even in the isolated cytoskeleton. In AFM, the system is not precise for size measurements. In addition, obtaining several images that allow a statistical value is difficult.

*Fast Fourier transform (FFT) analysis*

Images of the four distinct parabasal filaments and the costa were obtained by TEM and subjected to FFT analysis. Before image acquisition, samples were tilted using the goniometer to ascertain that the orientation of the filaments was perpendicular to the electron beam. It was achieved by recording images at angles where the filament bands presented the greatest distance. FFTs of selected areas of the filaments and the costa were autocorrelated using the FD Math tool in Fiji. Intensity profiles were obtained from each autocorrelation function (ACF), and the frequency of the filament bands was plotted. The following sequence was used: TEM image → Selected area of the PFs → FFT → Autocorrelation Function → density profile measurements.

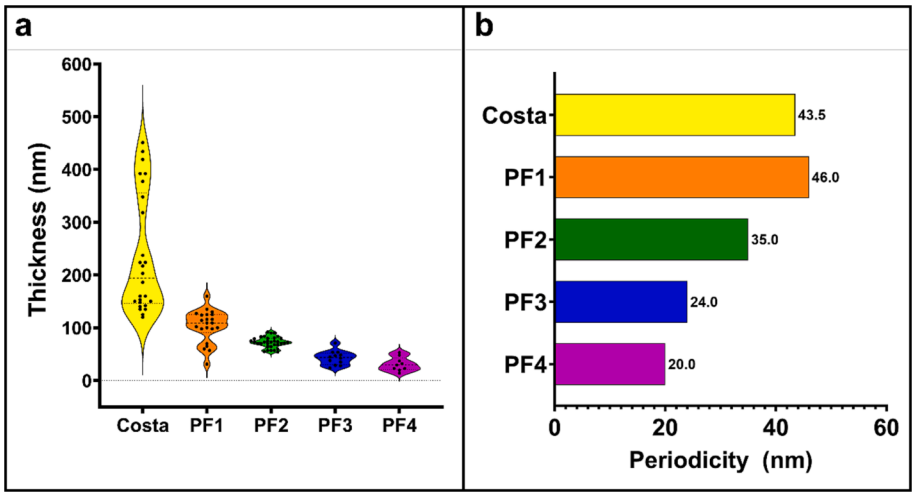


**Fig. 10.** In (a), a comparison of the thicknesses among the striated fibers of *T. vaginalis*. Notice that they have a large variation in thickness along their length. In (b), the striated fibers exhibit different periodicity in their bands. The measurements were carried out using the ZEISS Smart SEM software.

## Results and discussion

Scanning electron microscopy (SEM) has been used to analyze the surfaces of many cell types. However, until recently, the research was limited to the cell surface, gold coating, and low resolution when using most SEM.

Lee et al. (2009) showed 3D reconstruction images of *T. vaginalis* structures, revealing an additional parabasal filament. In addition, the authors claimed a split of the new parabasal filament designed as number 3. We employed high-resolution scanning microscopy (SEM), transmission electron microscopy (TEM), electron tomography (ET), and atomic force microscopy (AFM), which allowed us to visualize an extra parabasal filament, which was named PF4. We also analyzed the other striated fibers, including the costa and the PF1, PF2, and PF3, enabling measurement of the striation and determination of different patterns of each other.

### *Costa*

The costa (Fig. 1c, 2) is a rod-shaped striated structure found near the undulating membrane and extends towards the posterior region of the cell under the cell surface. *T. vaginalis* has a B-type costa, and its periodicity has been estimated at 42–60 nm (Honigberg and Brugerolle, 1990), depending on the preservation method used.

An earlier study (Honigberg and Brugerolle, 1990) claimed that in *T. vaginalis*, the longitudinal filaments are arranged in a "herringbone" pattern. They explained that this finding was based on alterations in the horizontal rows, where there is an alternation of direction in the adjacent horizontal rows at an angle to the longitudinal axis (Honigberg and Brugerolle, 1990).

A previous study stated that compared to other parabasal filaments, the costa is the longest and thickest of the striated filaments of T. *vaginalis* (Lee et al., 2009). We did not confirm this result (Fig. 1c, 2). Here, the longest striated fiber in *T. vaginalis* is PF1, which can be as long as 20 μm, depending on the whole cell size, whereas the costa size varies between 7 and 7.6 μm.

The costa has its origin in the basal body region, between the basal body (kinetosome) of the recurrent flagellum (R) (Fig. 1c) and kinetosomes #2 and #3 (De Andrade Rosa et al., 2017; Honigberg et al., 1971), and it is broader at the point at which it emerges. Here, we found that the initial costa region is wider and can reach 451 nm. It gradually thins until it reaches a thickness of 120 nm in some images. Thus, UHR-SEM becomes an obvious advantage as we can have a three-dimensional view of the structure along its entire length, which would be impossible with the traditional TEM and ultra-thin sections (Fig. 1b-c, 3a).

Previous studies performed with *Tritrichomonas foetus*, a cattle parasite, showed connections between the costa and the plasma membrane in the region of the undulating membrane, demonstrated by slam-freezing deep-etching (Benchimol et al., 1993).

In addition, in the study of De Andrade Rosa et al. (2013), the authors documented the existence of a novel accessory structure observed adjacent to the right-hand side of the costa in *T. foetus*. However, in *T. vaginalis*, this particular structure was not observed. The authors highlighted that the accessory filament exhibited a striated pattern akin to the costa, and this structure originated from locations with opposing orientations. Upon examination of the article's images related to the accessory filament, particularly Fig. 5a in the paper by De Andrade Rosa et al. (2013), it seems to resemble a parabasal filament running close to the costa, potentially leading to confusion with an accessory filament. The striation pattern of this accessory filament bears similarity to what we have observed in our current investigation regarding the parabasal filament. Nevertheless, in our images, we identified a distinct structure on the periphery of the costa, displaying an individualized pattern that we may consider as an accessory structure to the costa (Fig. 3). However, it deviates from the findings mentioned earlier in the context of *T. foetus*.

### *The parabasal filaments*

*T. vaginalis,* like all the Parabasalians, is characterized by the presence of the parabasal body, which is the Golgi complex or parabasal apparatus from where the phylum Parabasalia derives its name (Honigberg and Brugerolle, 1990). The *T. vaginalis* has a well-developed Golgi complex associated with the parabasal striated filaments originating near the basal bodies.

It has been assumed that *T. vaginalis* has three parabasal filaments: PF1, PF2, and PF3 (Honigberg and Brugerolle, 1990; Lee et al., 2009). The present work shows the discovery of an additional PF4 (Fig. 1c, 2). The PF1 arises between kinetosomes #2 and #3, whereas PF2 has a common origin with the costa's base and originates from kinetosomes #2 and R (from the recurrent flagellum) (Honigberg and Brugerolle, 1990). By tomography, Lee et al. (2009) demonstrated that PF1 is a long filament extending towards the posterior region of the cell, where it splits into two strands, one of which curves towards the interior of the cell from the split point. They have shown that PF1 and PF3 appeared to be very close to each other. However, in 1971, Honigberg et al. stated that PF1 could be seen as two or three separate structures. In our view, the authors observed the PF1, PF2, and PF3 in thin sections and interpreted them as one dividing filament.

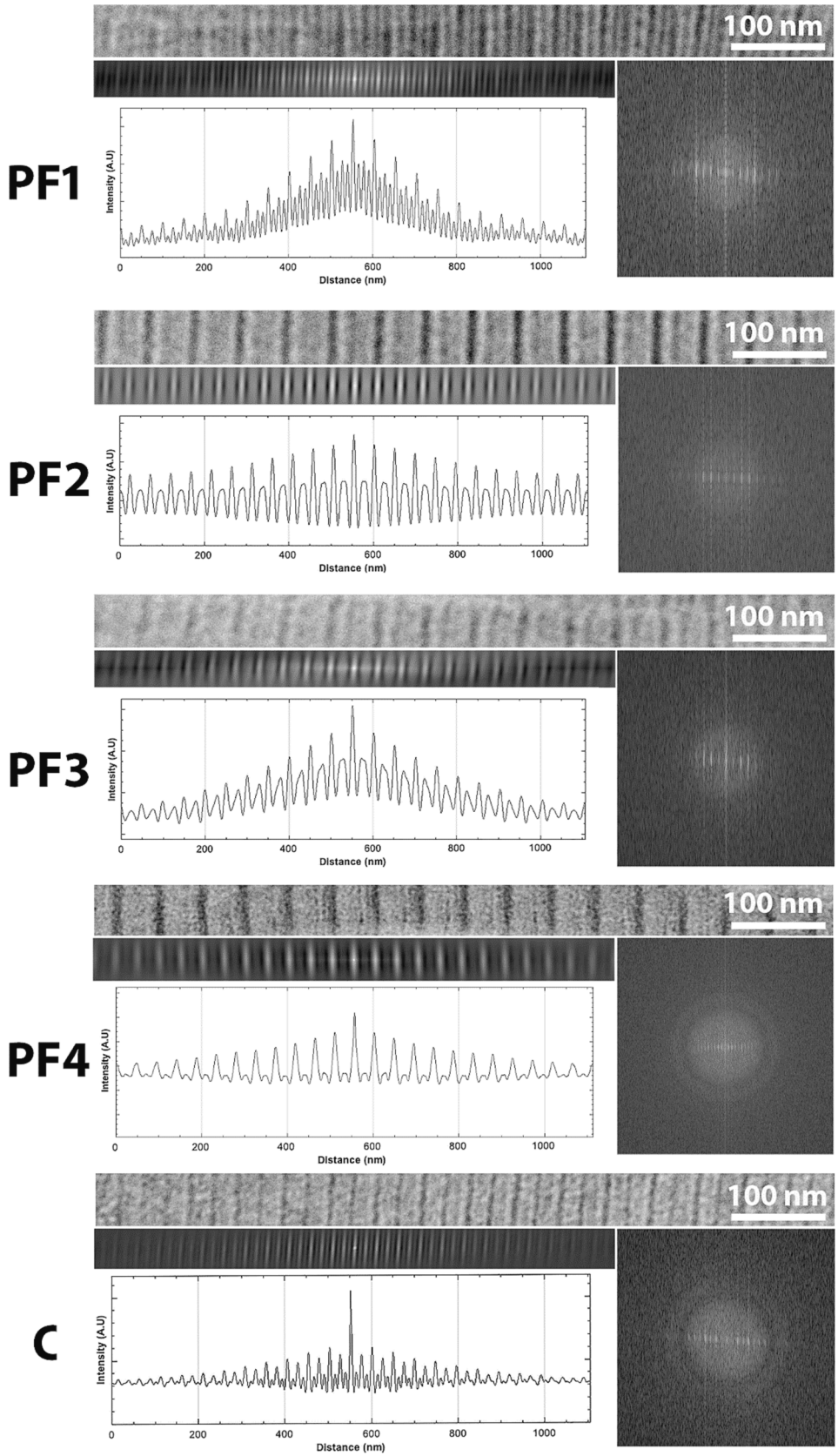


**Fig. 11.** Fast Fourier transforms (FFT) and autocorrelation profiles of PF1 to PF4 and the costa (C). The upper panel displays the selection of the TEM image used to generate the FFT (power spectrum of the frequency domain on the lower right). On the lower left below the micrograph are autocorrelation functions presented as an image and a profile plot. Notice the significant variations in the striation patterns between all the parabasal filaments and the costa.

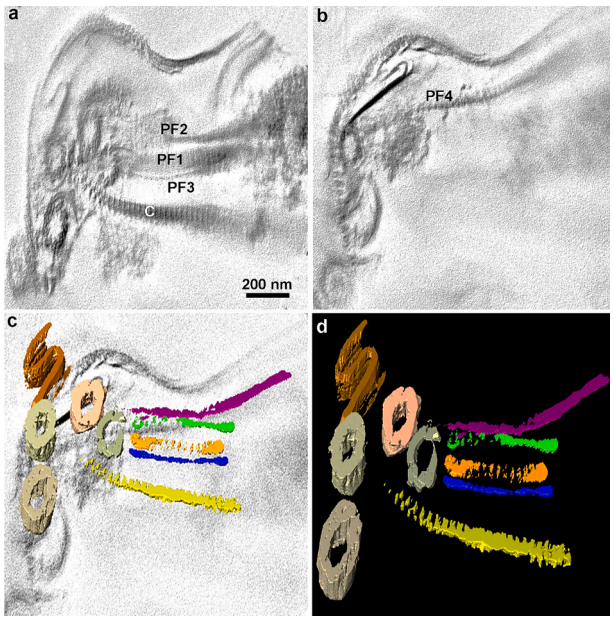


**Fig. 12.** TEM tomography of *T. vaginalis* cytoskeleton (a) This slice from a tomogram shows PF1, PF2, PF3, and costa, whereas in (b), PF4 appears. (c-d) A 3D model demonstrates the four parabasal filaments PF1 (orange), PF3 (blue), PF2 (green), PF4 (purple), the costa (yellow), the sigmoid filament (brown), and basal bodies (in shades of gray).

**Table 1**
Summary of the morphological data of the striated filaments of *T. vaginalis* obtained through 0.8 nm-resolution Scanning Electron Microscopy. PF, Parabasal filaments (1–4).

| Name | Length | Thickness (median) | Periodicity (mean) | Functions |
|---|---|---|---|---|
| **PF1** | 12–20 μm | 103 nm | 46 nm | Association with the *cis*-face of the Golgi complex |
| **PF2** | 5–6 μm | 70 nm | 35 nm | Association with the Golgi *trans*-face |
| **PF3** | 5–8 μm | 42 nm | 24 nm | Association with the Golgi *cis*-face |
| **PF4** | 2–4 μm | 31 nm | 20 nm | Association with the Golgi *trans*-face |
| **Costa** | 7–10 μm | 203 nm | 43,5 nm | Mechanical support for the undulating membrane and protection of the plasma membrane from shear forces generated by the movement of the recurrent flagellum |

All PFs originate in the kinetosome region near the costa's base (Fig. 1c, 2). Lee et al. (2009) reconstructed from serial sections *T. vaginalis* and, using tomographic reconstruction, showed the mastigont system and the parabasal filaments in detail. The authors reported that the new PF3 was close to the PF1 filament, and the two filaments appeared vertically parallel in the cross-sectional view. In addition, they claimed that this PF3 twisting of the split parabasal filament was seen after 3D reconstruction and electron tomography. It is important to mention that we did not section the structures here. Sectioning cells can lead to misinterpretations. To avoid sectioning and see the whole cell's structures, we used a high-resolution SEM (Fig. 2). This microscopy has a spectacular resolution. It avoids the gold coating, giving details of 0.8 nm of the resolution, which gives images of trichomonads that were not possible before by other methods. Thus, we noted that it was clear that both filaments (PF1 and PF3) run very close and parallel, and then the PF3 is slightly separate from the PF1 at a certain distance. In addition,

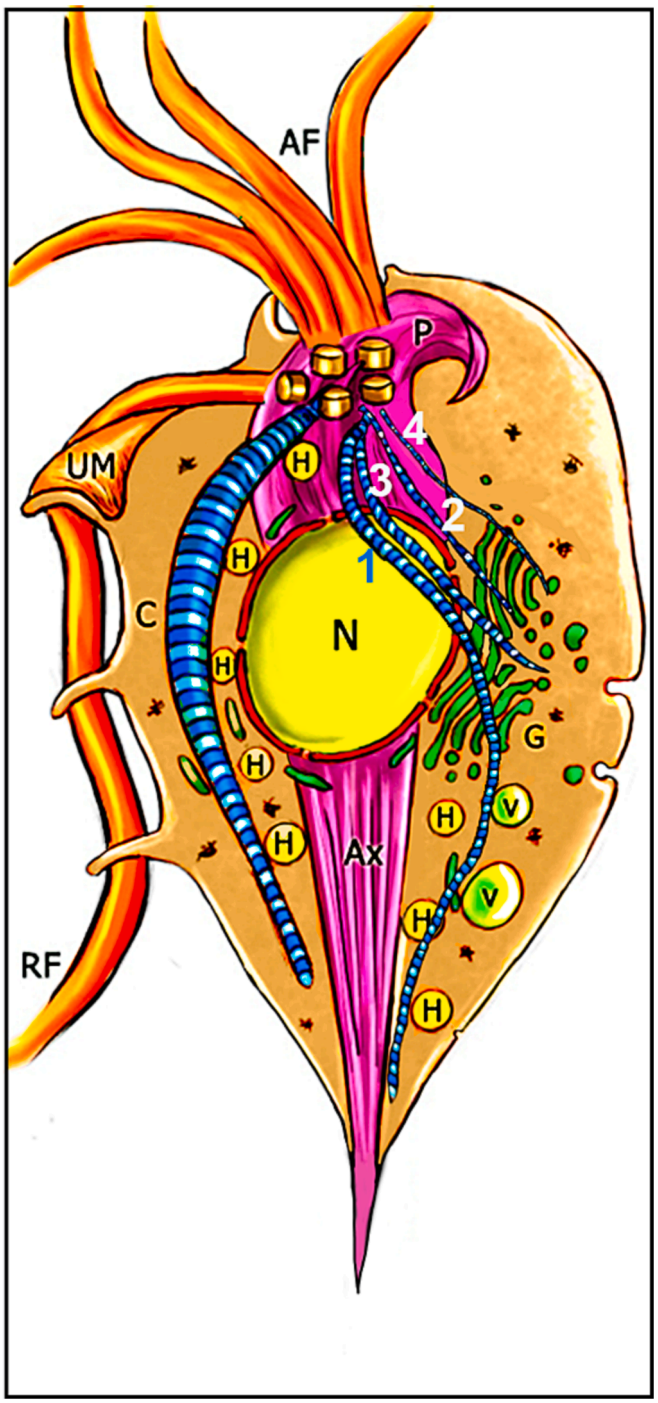


**Fig. 13.** Representative scheme of *T. vaginalis*. The four parabasal filaments were included. N, nucleus; C, costa, AF, anterior flagella; RF, recurrent flagellum; UM, undulating membrane; H, hydrogenosome; P, pelta; Ax, axostyle; G, Golgi; V, vacuole.

we did not observe the twisting. The PF3 is thinner and smaller than the PF1 and gradually tapers very thin (Fig. 2a-b, Fig. 6b).

The PF1 is the longest striated fiber, reaching the end of the cell, and it is the most common striated fiber, after the costa, observed in thin sections. Depending on the parasite's size, its length varied between 12 and 20 μm. Its thickness varied between 31 and 160 nm, with a median of 103 nm. However, it tapers and ends at its tip at just 31 nm thick. Its morphology differs from the costa's, presenting more rounded rings and a periodicity of about 46 nm (Figs. 2, 4). Interestingly, when observed from below, the striated fiber presents a different decoration (Fig. 4c).

Parabasal filament 2 (Fig. 5) runs parallel to PF4 (Fig. 1c, 2, 7), originates in the region of kinetosome # 2, and runs towards the Golgi for a distance between 2 and 3 μm. It passes through the Golgi between the the medial and trans cisternae (Fig. 2). It has a thickness of about 70 nm (between 54 nm and 92 nm) and a periodicity of 35 nm (Fig. 5).

The striated fiber PF3 runs closely to the PF1 (Fig. 1c, 2, 6). PF3 presents a thickness of 23.8 nm to 71 nm, with a median of 42 nm. Lee et al. (2009) claimed that PF1 splits into two strands, one of which curves towards the cell's interior from the split point. We do not find this result. The two filaments are very close and run adjacent until they separate. Lee et al. (2009) claimed that the bands in PF1 rotated horizontally from the split point, forming a twisting structure. Using UHR-SEM, we did not confirm this assumption.

Parabasal filament number 4 had not yet been visualized in any papers. Here, we observed it (Fig. 1c, 2, 7), which is very thin and short, and perhaps that is why it has not been described in articles that used ultra-thin sections in transmission electron microscopy. It could eventually be confused with one of the other filaments.

It has variable thickness; in its thickest region, it measures 53 nm and gradually thins out to measure 23 nm and, at the end, 14 nm. Its periodicity is 15 nm-25 nm (Figs. 7–9). Interestingly, this filament goes towards the Golgi in the *trans*-Golgi region (Fig. 2).

### *Atomic force microscopy (AFM)*

Previous studies in cell structures of *T. vaginalis* used thin sections for analyses in transmission electron microscopy or fixation, dehydration, drying, and gold coating for SEM. When cells are dehydrated and thin-sectioned, the research loses its 3-D view, and thus, laborious work must be made to reconstruct its view closest to the real natural image. The sample preparation for AFM imaging is more real since there is no need for stains, shadows, labels, or other procedures that could create artifacts in the material. In addition, an important advantage of AFM over EM is its ability to measure heights and obtain topographic maps of cells and subcellular structures. The AFM allows a new, impressive view of cells and organelles on a nanometer scale, including DNA observation on protozoa parasites (Cavalcanti and De Souza, 2018).

Here, to complement our TEM and SEM studies, we used AFM in a liquid medium with no dehydration or resin embedding to get a more natural view of the striated fibers in *T. vaginalis*. Our research group successfully analyzed each parabasal filament, comparing its pattern with the costa, another striated filament of *T. vaginalis* (Fig. 9). We obtained a spectacular view of the four parabasal filaments and the costa. However, despite obtaining good images, this equipment is very slow in obtaining each image and is not suitable for providing size measurements. Therefore, we only use it to complement the visualizations obtained with other methods and not for statistical analysis. Thus, we could compare the different patterns among all striated fibers and get a more realistic image of these cell structures for the first time. Each fiber is distinct concerning its morphology, thickness, periodicity, and position in the cell.

### *Periodicity of striated filaments*

In the early literature, the term parabasal apparatus was applied to both PF1 and PF2, which are associated with the Golgi complex. It is believed that PFs accompany the Golgi, and thus, their function would be to support the Golgi complex (Honigberg and Brugerolle, 1990), although no clear evidence exists for this assumption. The parabasal filaments may play an important role in preserving the integrity of the trichomonad cell by connecting the kinetosomes and other parts of the cell, including the Golgi apparatus.

These two filaments present, at first glance, identical periodicity to that of the costa that involves alternating transverse electron-dense and electron-lucent regions, and the dense area consists of four thin, dense lines (Honigberg and Brugerolle, 1990); however, we noted that in PFs the band pattern is distinct when compared with the costa, although presenting a periodic structure (Figs. 8, 9, 10b-11). Using the negative staining and analyzing by TEM allowed a very good observation of the different striation patterns among the fibers (Fig. 8), which was corroborated by the other methods, such as atomic force microscopy and UHR-SEM.

In addition, in *T. foetus,* the parabasal filaments were described as thinner striated fibers (128.5 ± 9.6 nm) and shorter than the costa and their periodicity (40.2 ± 5.4 nm) described as similar to the costa (De Andrade Rosa et al., 2013). In the present study with *T. vaginalis,* we found the opposite. The periodicity of the PF filaments is distinct from the costa (Figs. 10 and 11), and each parabasal filament presents a distinct thickness (Fig. 10a).

Fast Fourier Transformation (FFT) analysis of TEM images revealed significant variations in the striation patterns among different filaments and the costa. Plot profiles derived from images deconvolved using correlated FFTs indicated that PF1 and the costa (Fig. 11) exhibit the shortest striated banding pattern. In contrast, the striation pattern appears more spaced in parabasal filaments PF2, PF3, and PF4 (Fig. 11).

As mentioned above, when compared to regular TEM, SEM analysis of cytoskeleton elements from membrane-extracted cells presents several advantages. It allows for the analysis of the entire volume of the structures, as opposed to the thin sections typically covering only a fraction of their volume and potentially having any orientation. To accurately assess the striated banding patterns in different PFs and the costa, whether through direct measurements in calibrated TEM images or FFT analysis, it is crucial to ascertain the correct sample orientation before image acquisition. It can be achieved by tilting the samples in the TEM to ensure that the filament bands exhibit the greatest distance. Additionally, since different density variations may arise from direct intensity profile measurements on TEM images, potentially leading to interpretation difficulties, one approach to assessing the banding pattern is by computing the Fourier transform, which reveals the periodicities within the selected image areas. Computing the autocorrelation function enhances the variation in the banding pattern as well as providing a vehicle for comparing quantitatively the different filaments (Fig. 11).

### *Golgi relationships and the parabasal filaments*

The literature describes the PFs as located above the nucleus and below the well-developed Golgi complex in trichomonads (Fig. 2 a-b, 13). Here, we found that two PFs (PF1 and PF3) are at the cis Golgi region, whereas the PF2 and PF4 are in the *trans*-Golgi. These positions would help the correct distribution of the cisternae to the next daughter cells since the Golgi complex in trichomonads is an extensively developed organelle. Before the cell division, it doubles in size and does not fragment during mitosis (Benchimol et al., 2001). The *T. vaginalis* Golgi is involved in the synthesis of important adhesive molecules (adhesins) that contribute to interactions between *T. vaginalis* and host-epithelial cells (Arroyo et al., 1993) in $Ca^{++}$ regulation, protein and carbohydrate processing, and lysosomes biogenesis (Benchimol et al., 2001), which would justify its large size. In addition, the authors demonstrated that a parabasal filament is seen connected to the first cisternae of the Golgi complex by thin filaments.

Preisner et al. (2016) reported the proteomic profiling of the detergent-resistant components of the cytoskeleton of *T. gallinarum,* demonstrating that the majority of identified proteins lack homologs outside of the Trichomonadidae and are unique to this group of protists. They identified homologs of *T. vaginalis* and localized five such homologs of cytoskeleton proteins that share features of intermediated filaments reminiscent of metazoan cells. It is important to mention that in other protists, such as the flagellated *Ochromonas,* the Golgi complex remains supported by a striated fiber originating in the basal body complex, which was clearly shown to act as a microtubule-organizing center (MTOC) orienting spindle pole formation during mitosis (Bouck and Brown, 1973). Thus, in trichomonads, in attempting to consider that

PFs and Golgi connection is important and could participate in other functions. Future studies are needed to add more knowledge in this area.

Although TEM allows important information concerning the cells, the images of the sample must be thin enough for electrons to pass through. Typically, sections are made very thin (50–100 nm); thus, the cell and substructures in 3-D image configuration are lost. The parabasal filaments are thin structures, and it is difficult to get images of more than one PF in a lucky section of *T. vaginalis*. In addition, examining whole, cross-sectioned cells could potentially lead to misinterpretations. Because of this, at the beginning of studies on the cell biology of trichomonads, a controversial number of the PFs was published (Čepička et al., 2016). Lee et al. (2009) found a third PF using EM tomography. Here, we used a diverse range of scanning probe microscopy techniques complemented by electron tomography (EM). To get deeper images of the parasite, we prepared isolated *T. vaginalis* cytoskeletons. We obtained thick sections (about 200 to 300 nm), and a series of TEM images from the same sample was collected through a range of angles, from which a 3D image could be reconstructed. We looked for all striated fibers at different planes. Thus, we created 3D representations revealing the presence of the four parabasal filaments. Nevertheless, we successfully visualized the filaments within a specific plane by isolating an enriched fraction of the cytoskeletal components and conducting a thorough analysis (Fig. 12) and new insights into the trichomonads ultrastructure that could not be obtained from two dimensions alone. Starting from the tomographic reconstruction, we created a 3D model showing the composition of the basal bodies, sigmoid, costa, and the four parabasal filaments (Fig. 12c-d), and a movie of the tomography was added as supplemental material.

The tomography analysis was important to visualize the arrangement of the four filaments, corroborating the scanning microscopy images. We note that in the basal planes, we visualize PF1, PF2, PF3, and costa (Fig. 12a), and in another plane using tomographic reconstruction, we can notice PF4 (Fig. 12b).

Movie 1. Electron tomography of *T. vaginalis* cytoskeleton. Translation through the virtual slices shows filaments in different planes. The 3D reconstruction revealed four filaments parabasal filaments, PF1 (orange), PF3 (blue), PF2 (green), PF4 (purple), the costa (yellow), the sigmoid filament (brown), and basal bodies (in shades of gray).

## Conclusion

In this study, we have investigated the cytoskeleton of *T. vaginalis*, a urogenital parasite, using a diverse range of scanning probe microscopy techniques, which were complemented by electron tomography and Fast-Fourier methods. This multi-modal approach has allowed us to characterize an unknown parabasal filament and reveal the ultrastructure of other striated fibers that have not been published before (Table 1). We present a scheme showing the cell structure of *T. vaginalis* with all striated fibers (Fig. 13). This knowledge will contribute to a better understanding of this important parasite.

## Funding

This work has been supported by Conselho Nacional de Desenvolvimento Científico e Tecnológico-CNPq, Fundação Carlos Chagas Filho de Amparo à Pesquisa do Estado do Rio de Janeiro (GRANT number E-26/200.956/2021), Funadesp and Financiadora de Estudos e Projetos (FINEP).

## CRediT authorship contribution statement

**Sharmila Fiama das Neves Ortiz:** Methodology, Visualization, Writing – review & editing. **Raphael Verdan:** Investigation, Methodology, Writing – review & editing. **Gustavo Miranda Rocha:** Formal analysis, Investigation, Methodology, Writing – review & editing. **Kildare Miranda:** Data curation, Investigation, Methodology, Software, Validation, Writing – original draft, Writing – review & editing. **Marlene Benchimol:** Conceptualization, Data curation, Formal analysis, Funding acquisition, Investigation, Methodology, Project administration, Resources, Supervision, Validation, Visualization, Writing – original draft, Writing – review & editing.

## Declaration of competing interest

The authors declare that they have no known competing financial interests or personal relationships that could have appeared to influence the work reported in this paper.

## Data availability

Data will be made available on request.

## Acknowledgments

We thank Fundação Carlos Chagas de Amparo a Pesquisa do Estado do Rio de Janeiro (GRANT number E-26/200.956/2021Vânia da Silva Vieira for technical support in the Auriga microscopy.

## Appendix A. Supplementary data

Supplementary data to this article can be found online at https://doi.org/10.1016/j.yjsbx.2024.100099.

## References

Arroyo, R., Gonzalez-Robles, A., Martinez-Palomo, A., Alderete, J.F., 1993. Signalling of *Trichomonas vaginalis* for amoeboid transformation and adhesion synthesis follows cytoadherence. Mol. Microbiol. 7, 299–309. https://doi.org/10.1111/j.1365-2958.1993.tb01121.x.

Benchimol, M., 2004. Trichomonads under microscopy. Microsc. Microanal. 10 (5), 528–550. https://doi.org/10.1017/S1431927604040905.

Benchimol, M., Kachar, B., de Souza, W., 1993. The structural organization of the pathogenic protozoan *Tritrichomonas foetus* as seen in replicas of quick frozen, freeze-fractured and deep etched cells. Biol. Cell 77 (3), 289–295. https://doi.org/10.1016/s0248-4900(05)80200-x.

Benchimol, M., Ribeiro, K.C., Mariante, R.M., Alderete, J.F., 2001. Structure and division of the Golgi complex in *Trichomonas vaginalis* and *Tritrichomonas foetus*. Eur. J. Cell Biol. 80, 593–607. https://doi.org/10.1078/0171-9335-00191.

Bouck, B.G., Brown, D.L., 1973. Microtubule biogenesis and cell shape in *Ochromonas*. I. the distribution of cytoplasmic mitotic microtubules. J. Cell Biol. 56, 340–359.

Brown, J.R., Schwartz, C.L., Heumann, J.M., Dawson, S.C., Hoenger, A., 2016. A detailed look at the cytoskeletal architecture of the *Giardia lamblia* ventral disc. J. Struct. Biol. 194, 38–48. https://doi.org/10.1016/j.jsb.2016.01.011.

Cavalcanti, D.P., de Souza, W., 2018. The kinetoplast of trypanosomatids: from early studies of electron microscopy to recent advances in atomic force microscopy. Scanning 2018, 9603051. https://doi.org/10.1155/2018/9603051.

Čepička, I., Dolan, M.F., Gile, G.H., 2016. Parabasalia. In: Archibald, J., *et al.* Handbook of the Protists. Springer, Cham. https://doi.org/10.1007/978-3-319-32669-6_9-1.

De Andrade Rosa, I., de Souza, W., Benchimol, M., 2013. High-resolution scanning electron microscopy of the cytoskeleton of *Tritrichomonas foetus*. J. Struct. Biol. 183, 412–418.

De Andrade Rosa, I., Caruso, M.B., de Oliveira Santos, E., Gonzaga, L., Zingali, R.B., de Vasconcelos, A.T.R., de Souza, W., Benchimol, M., 2017. The costa of trichomonads: a complex macromolecular cytoskeleton structure made of uncommon proteins. Biol. Cell 109, 238–253. https://doi.org/10.1111/boc.201600050.

De Souza, W.D., Cunha-e-Silva, N.L.D., 2003. Cell fractionation of parasitic protozoa: a review. Mem. Inst. Oswaldo Cruz 98, 151–170. https://doi.org/10.1590/S0074-02762003000200001.

Diamond, L.S., 1957. The establishment of various trichomonads of animals and man in axenic cultures. J. Parasitol. 43 https://doi.org/10.2307/3274682.

Dvorak, J.A., Kobayashi, S., Abe, K., Fujiwara, T., Takeuchi, T., Nagao, E., 2000. The application of the atomic force microscope to studies of medically important protozoan parasites. J. Electron Microsc. (Tokyo) 49 (3), 429–435. https://doi.org/10.1093/oxfordjournals.jmicro.a023825.

Honigberg, B.M., Brugerolle, G., 1990. Structure. In: Trichmonads Parasitic in Humans. Springer-Verlag, New York, pp. 5–35.

Honigberg, B.M., Mattern, C.F., Daniel, W.A., 1971. Fine structure of the mastigont system in Tritrichomonas foetus (riedmüller). J. Protozool. 18, 183–198. https://doi.org/10.1111/j.1550-7408.1971.tb03306.x.

Lee, K.E., Kim, J.H., Jung, M.K., Arii, T., Ryu, J.S., Han, S.S., 2009. Three-dimensional structure of the cytoskeleton in *Trichomonas vaginalis* revealed new features. J. Electron Microsc. (Tokyo) 58, 305–313. https://doi.org/10.1093/jmicro/dfp019.

Preisner, H., Karin, E.L., Poschmann, G., Stühler, K., Pupko, T., Gould, S.B., 2016. The cytoskeleton of parabasalian parasites comprises proteins that share properties common to intermediate filament proteins. Protist 167, 526–543.

Ribeiro, K.C., Monteiro-Leal, L.H., Benchimol, M., 2000. Contributions of the axostyle and flagella to closed mitosis in the protists *Tritrichomonas foetus* and *Trichomonas vaginalis*. Euk. Microbiol. 47, 481–492.

Rocha, G.M., Miranda, K., Weissmüller, G., Bisch, P.M., de Souza, W., 2010. Visualization of the flagellar surface of protists by atomic force microscopy. Micron 41 (8), 939–944. https://doi.org/10.1016/j.micron.2010.07.007.

Trépout, S., Tassin, A.M., Marco, S., Bastin, P., 2018. STEM tomography analysis of the trypanosome transition zone. J Struct Biol, 202(1), 51–60. .

Vidal, J.C., Alcantara, C.L., de Souza, W., Cunha-E-Silva, N.L., 2016. Loss of the cytostome-cytopharynx and endocytic ability are late events in *Trypanosoma cruzi* metacyclogenesis. J. Struct. Biol. 196 (3) https://doi.org/10.1016/j.jsb.2016.07.018.

Viscogliosi, E., Brugerolle, G., 1994. Striated fibers in trichomonads: costa proteins represent a new class of proteins forming striated roots. Cell Motil. Cytoskeleton 29 (1), 82–93. https://doi.org/10.1002/cm.970290108.